Journal of Fluids and Structures (2001) **15,** 659–669
doi:10.1006/jfls.2000.0359, available online at http://www.idealibrary.com on IDEAL®

NUMERICAL PREDICTION OF VIV ON LONG FLEXIBLE CIRCULAR CYLINDERS

R. H. J. Willden and J. M. R. Graham

Department of Aeronautics, Imperial College of Science, Technology and Medicine London, SW7 2BY, U.K.

(Received 5 September 2000, and in final form 14 December 2000)

Two-dimensional and quasi-three-dimensional numerical methods have been employed to simulate the vortex-induced vibrations of a circular cylinder. A low Reynolds number two-dimensional study at low mass ratio and zero damping revealed lock-in across a large range of reduced velocities. For the low mass ratio cylinder simulated, the oscillatory frequency was found to be controlled by the fluid via its added mass. Oscillations far from the body's natural frequency were observed. The shear stress contributions to the transverse force acting on the body were very significant and play an important role in the dynamics of low Reynolds number vortex-induced vibrations. The quasi-three-dimensional method was employed to simulate the flow past a long stationary cylinder in shear flow. Cellular shedding was observed in its wake. The free transverse flexible vibrations of the same body exhibited significant spanwise correlation over a large length of the body despite the sheared inflow.

1. INTRODUCTION

Riser pipes are long flexible, substantially vertical, circular cylinders used in the offshore industry to convey fluids from the sea bed to sea level and *vice-versa*. For exploration in ultra deep waters, risers of up to 2000 m length, yielding aspect ratios of order 10^3, have been proposed. The Reynolds number associated with these flows is typically of order 10^5.

Flexibly supported cylinders may undergo vortex-induced vibrations, through which the vortex-shedding frequency may lock on to a frequency of vibration of the structure. The range over which lock-in occurs depends on the vibration amplitude and on the mass and damping ratios. Flow-induced vibrations are a multiple-degree-of-freedom problem, in which coupling exists between motions in-line with and transverse to the stream. The amplitude of transverse oscillations can be of the order of one diameter and therefore present a potent source of fatigue as well as the possibility of clashing in multiple-cylinder assemblies.

Risers can be subject to currents with significant shear profiles, giving rise to large variations in the vortex-shedding frequency with depth. At any one depth the mode of vibration closest in frequency to the local natural vortex shedding frequency is the most likely to be excited. However, the influence of other modes of vibration excited by the current at other depths may result in constructive or destructive interference.

The vortex-induced vibrations of rigid cylinders have recently received renewed attention. In particular the multiple branching behaviour and hysteresis effects observed for the amplitude of free transverse vibrations of a circular cylinder at low mass and damping ratios have been the focus of many works (Brika & Laneville, 1995; Khalak & Williamson, 1999; Newman & Karniadakis, 1995). Due to the high aspect ratios of riser pipes, three-dimensional flow simulations at realistic Reynolds numbers are still considered infeasible. Lucor

0889–9746/01/040659 + 11 $35.00/0

et al. (2000) have simulated the flow over a flexible cable of aspect ratio 567, subject to a sheared current with a peak Reynolds number of 1000, a long way short of the values required for full riser computations.

Consequently, approximate techniques such as strip theory (Herfjord *et al.* 1999) have been used to simulate riser response. The technique employed in the present work is a quasi-three-dimensional extension of strip theory. A two-dimensional hybrid Eulerian/Lagrangian Navier–Stokes code (Graham 1988) is used to simulate the flow around several spanwise sections of the riser. These are linked hydrodynamically through a three-dimensional large-scale vortex lattice representation of the wake (Giannakidis & Graham 1997). A three-dimensional structural dynamics model is coupled to the fluid solver so as to predict the response.

The work presented here focuses on the flow-induced transverse vibrations of a rigid two-dimensional low mass cylinder, elastically mounted with zero damping, so as to excite a large response, and on the transverse vibrations of a long flexible cylinder in sheared flow.

2. SIMULATION METHOD

The two-dimensional Navier–Stokes solver and its quasi-three-dimensional extension are briefly described below along with the structural dynamics models and the fluid–structure interaction procedure. For a more detailed account see Willden & Graham (2000).

2.1. Fluid Dynamics Models

A first-order simulation is used to solve the two-dimensional incompressible Navier–Stokes equations in their velocity–vorticity formulation:

$$\frac{\partial \omega_z}{\partial t} + (\mathbf{u}\cdot\nabla)\omega_z = \nu\nabla^2\omega_z, \tag{1}$$

where ω_z is the spanwise vorticity component. A time-split approach is followed, whereby the diffusion of vorticity is treated in an Eulerian fashion by modelling the flow variables using linear finite element approximations on an unstructured mesh, and the convection is handled using a Lagrangian approach that employs discrete point vortices. The velocity field is evaluated through the finite element solution of the two-dimensional derivative of the Poisson equation relating velocity and vorticity:

$$\nabla^2\mathbf{u} = -\nabla\wedge\boldsymbol{\omega}. \tag{2}$$

The Poisson equation relating pressure to velocity (divergence of the momentum equations), is solved using the finite element method to yield the pressure components of the body forces. Those due to viscous shear stresses at the wall, τ_w, are computed from the vorticity at the wall, according to $\tau_w(s) = -\mu\omega_z(s)$, where s defines the tangent to the wall.

In three dimensions, multiple two-dimensional computational planes are placed along the cylinder span. These are linked hydrodynamically using an inviscid unsteady three-dimensional vortex lattice. The lattice is constructed so as to represent the three-dimensional vorticity field. This is done by updating its spanwise vorticity content from the underlying two-dimensional vorticity fields. The remaining vorticity components are deduced by constructing the lattice so as to be divergence free. The lattice is allowed to self-convect over the step. Once a part of the lattice passes the downstream extremities of the computational planes it can no longer be up-dated and is allowed to self-convect and distort into the far wake. The Biot–Savart law is used to retrieve velocity information from

the lattice, including $\partial w/\partial z$, the spanwise derivative of the spanwise velocity component. This provides a source term in the sectional solution of equation (2), which allows mass conservation in three dimensions to be retained. The far-field velocity boundary conditions of the computational planes are modified to include the velocities induced by the lattice.

2.2. Structural Dynamics Models

A spring-mass-damper model is used to simulate the single-degree-of-freedom transverse vibration of a two-dimensional cylinder. The equation of motion for the cylinder displacement, y, in response to fluid loading, represented by the lift coefficient C_L, is given by

$$m\frac{\mathrm{d}^2y}{\mathrm{d}t^2} + 2\beta m(2\pi f_n)\frac{\mathrm{d}y}{\mathrm{d}t} + m(2\pi f_n)^2 y = C_L(t)\frac{\rho U^2}{2}D, \tag{3}$$

where m, f_n and β are the mass of the cylinder per unit length, the natural frequency of cylinder vibration and the fraction of critical viscous damping respectively; U, ρ and D are the upstream velocity, the density of the fluid and the cylinder diameter, respectively.

The three-dimensional flexible cylinder is modelled as a bending beam under pre-tension using a linear finite element implementation of the Bernoulli–Euler beam equations. The model permits three degrees of freedom at each of the finite element nodes, axial and transverse displacements and a rotation about an axis normal to the plane of the displacements. The model incorporates tension, buoyancy and gravity but neglects structural damping.

The response of the cylinder to the fluid loading is calculated explicitly by both structural dynamics models. The fluid dynamics is subsequently solved implicitly.

3. RESULTS & DISCUSSION

3.1. Two-dimensional Free Transverse Vibrations of a Flexibly Mounted Cylinder

The response of a circular cylinder free to vibrate in the transverse direction has been computed over a range of reduced velocities, $V_r = U/f_nD$, from 2·5 to 16. The simulations were performed on a continuous basis by incrementing the Reynolds number in small positive steps, starting with the cylinder at rest at $\mathrm{Re} = 50$ ($V_r = 2{\cdot}5$) and terminating at $\mathrm{Re} = 320$ ($V_r = 16$). The purpose of this was to ensure that the simulations incorporated any fluid memory effects that may be seen experimentally with increasing flow speed. The mass and damping ratios, $m^* = 2m/\rho D^2$ and β, of the cylinder are 1 and 0 respectively.

The nondimensional response amplitude, A/D, is shown in Figure 1 over the range of V_r simulated. The response amplitude at the start of the simulation, $V_r = 2{\cdot}5$, is $0{\cdot}02D$. Relatively small amplitude oscillations are maintained until $V_r = 3{\cdot}1$, after which the response increases markedly with V_r. The increasing response amplitude starts to saturate at $V_r = 4{\cdot}7$ at an amplitude of $0{\cdot}47D$. It is not until $V_r = 6{\cdot}1$ that the response peaks at $0{\cdot}50D$. This amplitude is approximately maintained until the end of the simulation at $V_r = 16$. Although the flow past a circular cylinder is considered to be three-dimensional past a Reynolds number of approximately 190, the simulation was continued past this point, $V_r = 9{\cdot}5$, on the premise that lock-in has two-dimensionalizing effects.

The oscillatory and vortex-shedding frequencies are defined as f_o and f_v respectively, with $f_o = f_v$ at lock-in. It is apparent that at this low mass ratio the oscillatory and vortex-shedding frequencies remain locked-in to one another throughout the V_r range simulated. f_o/f_n (Figure 1) does not display the step at $f_o/f_n \approx 1$ that characterizes lock-in for moderate to high mass ratios. Instead, the variation in f_o is close to linear and varies from $0{\cdot}29f_n$ at the

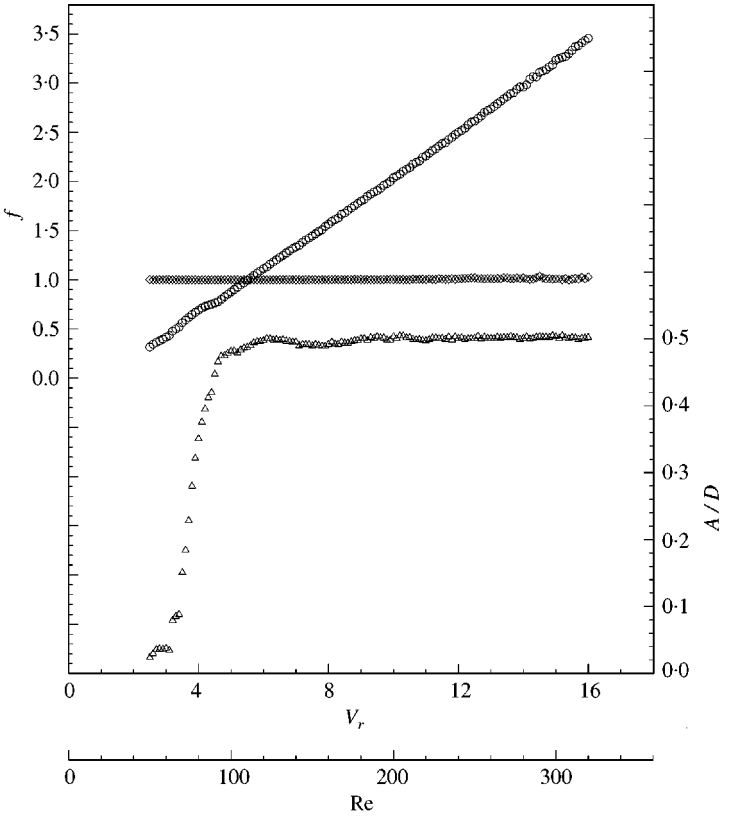

Figure 1. Amplitude and frequencies of a circular cylinder vibrating freely in the transverse direction for $m^* = 1$, $\beta = 0$: $\triangle$, A/D; $\bigcirc$, f_o/f_n; $\diamond$, f_o/f_N.

start of the simulation to $3{\cdot}45f_n$ at its end. This infers that for this very low mass ratio, the fluid is dominant over the structure in controlling the oscillatory frequency throughout lock-in. The reverse of this is true where the lock-in step is observed.

The ability of the structure to oscillate far from its natural frequency is better understood by considering the role of the added mass, $m_a = \hat{L}/A(2\pi f_o)^2$, where $\hat{L}$ is the amplitude of the component of the fluctuating lift force in phase with body displacement. Zero structural damping infers that $\hat{L}$ is necessarily the amplitude of the total fluctuating lift force; hence, $L(t) = \hat{L}\sin(2\pi f_v t)$. This definition of m_a allows equation (3), in the absence of damping, $\beta = 0$, and for the case of lock-in, $f_o = f_v$, to be written as

$$(m + m_a)\frac{\mathrm{d}^2 y}{\mathrm{d}t^2} + m(2\pi f_n)^2\, y = 0, \tag{4}$$

where $y(t) = A\sin(2\pi f_o t)$. An effective natural frequency of the combined fluid and structure system, f_N, may be defined according to $f_N^2 = f_n^2/(1 + m_a/m)$. Non-dimensionalizing f_o by f_N reveals that the body oscillates at or very close to f_N throughout lock-in (Figure 1).

The ratio m_a/m describes the relative magnitudes of the fluid and body inertia forces. At high values of this ratio the body behaves as if it is controlled by a forced motion at the vortex-shedding frequency. At low values the body oscillates near its natural frequency. Figure 2 displays m_a/m against f_o/f_n for the simulated data. At the start of the simulation

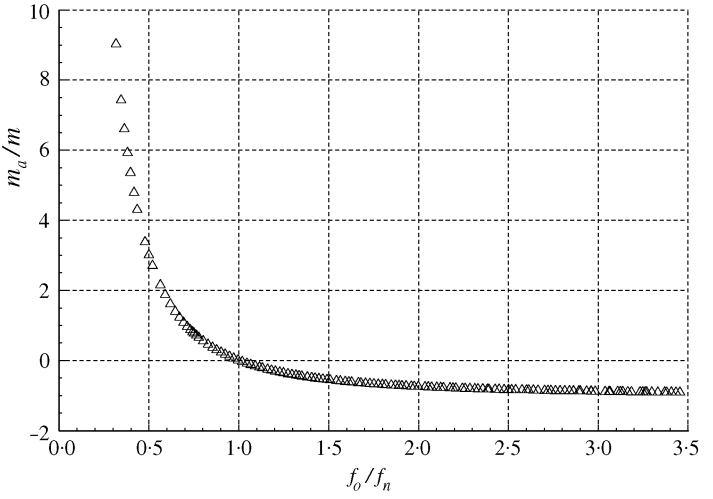

Figure 2. The added mass, m_a, of a circular cylinder vibrating freely in the transverse direction for $m^* = 1$, $\beta = 0$.

m_a/m peaks at 9·03. The added mass rapidly decreases with increasing V_r until it reaches zero, somewhere between $V_r = 5{\cdot}5$ and 5·6, at which point the body is free to oscillate at its natural frequency, $f_o/f_n = 1$. Past this point, the added mass becomes negative as the lift force moves out of phase with the displacement. As V_r is increased still further, m_a/m asymptotes to a value close to -1; the minimum value achieved is $-0{\cdot}91$ at $V_r = 16$.

Figure 3 depicts a selection of vortex particle images of the wake of the oscillating cylinder along with corresponding time traces of response, lift and drag coefficients, y/D, C_L and C_D, respectively. Also shown are time traces, over different time periods for clarity, of the contributions to C_L by pressure forces and shear stresses, C_{Lp} and C_{Lf} respectively.

This figure depicts simulations at $V_r = 3{\cdot}9$, where $C_L(t)$ is in phase with $y(t)$, at $V_r = 5{\cdot}5$, approximately at the phase change, and at $V_r = 10.0$, where $C_L(t)$ is in anti-phase with $y(t)$. The shedding in all cases is of the 2S type. The increasing oscillatory amplitude with V_r is responsible for a breakdown in the stability of the von Kármán street due to larger transverse separations between vortices. Consequently the staggered vortex wake has to readjust itself in the middle-wake region, by rolling up and coalescing like signed pairs of vortices to form larger vortex structures, as depicted in the wake images for $V_r = 5{\cdot}5$ and 10·0. The time traces for these two cases show slight modulations for which the frequencies are given by the differences in the frequencies of the near- and far-wake vortex structures.

The in-phase and anti-phase nature of y/D and C_L are best observed for cases $V_r = 3{\cdot}9$ and 10·0, respectively. Less clear is the relative phase of the traces for $V_r = 5{\cdot}5$ which is made more complex by higher frequencies. A small phase difference between the pressure and shear stress contributions to C_L can be observed for $V_r = 3{\cdot}9$. Both are approximately in phase with y/D. For the case just prior to the phase change, $V_r = 5{\cdot}5$, there is a phase difference of approximately 180° between C_{Lp} and C_{Lf}; C_{Lp} is in anti-phase with the displacement whilst C_{Lf} remains in phase. This phase difference between C_{Lp} and C_{Lf} persists until the end of the simulation at $V_r = 16$, as shown in the traces for $V_r = 10{\cdot}0$.

Much of this information is summarized by Figure 4. The high relative magnitude of C_{Lf} with respect to C_{Lp}, in particular before the phase change ($f_o = f_n$), is evident. The pressure contribution on its own changes phase with respect to the response between $V_r = 4{\cdot}8$ and 4·9. The peak in the overall lift coefficient occurs at $V_r = 3{\cdot}9$ some way short of

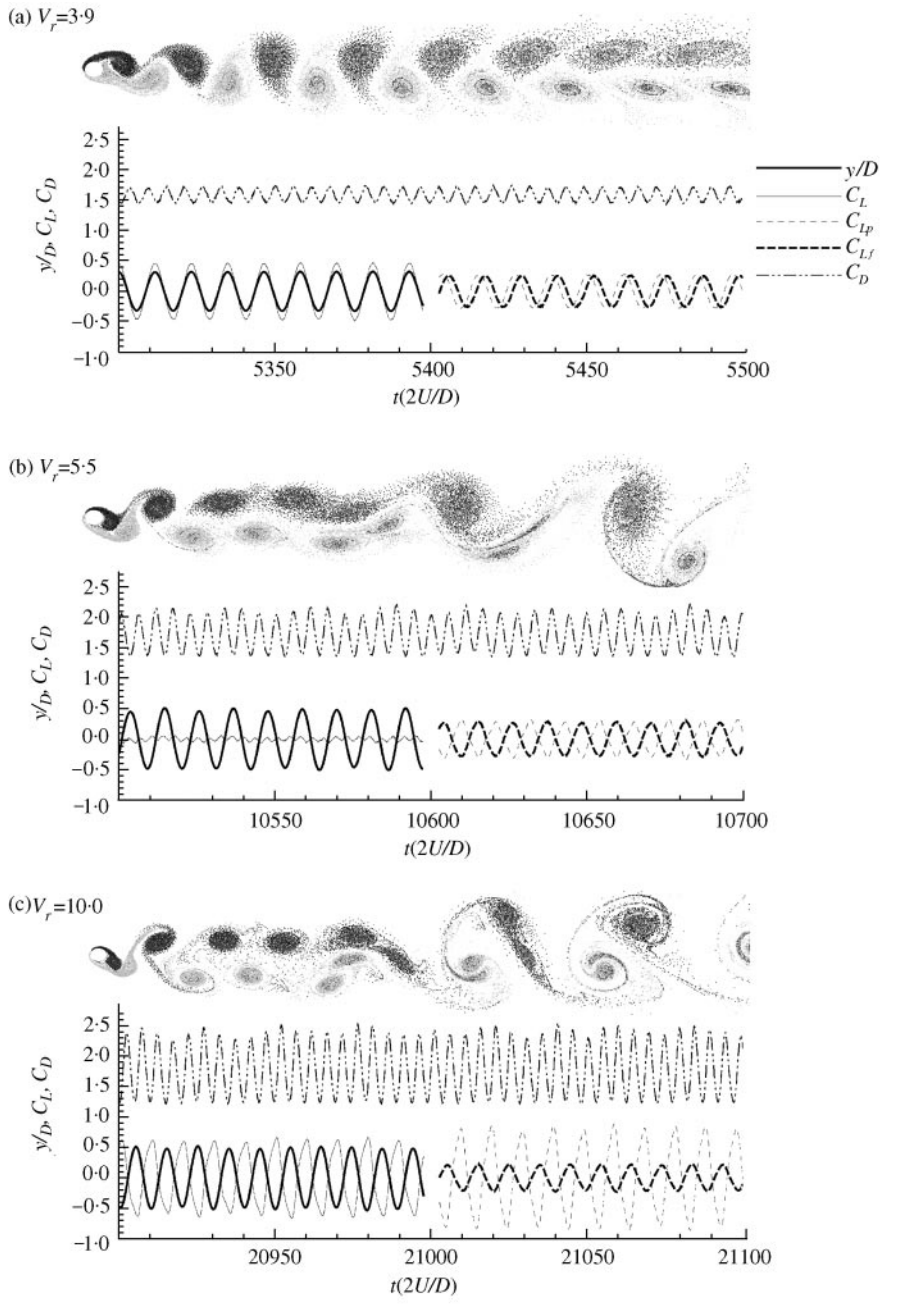

Figure 3. Particle images of the wake, response, lift and drag coefficient (y/D, C_L and C_D) histories of a circular cylinder vibrating freely in the transverse direction; $m^* = 1$, $\beta = 0$, at reduced velocities, (a, b, c) $V_r = 3{\cdot}9$, $5{\cdot}5$ and $10{\cdot}0$.

the V_r of the maximum response amplitude. This is in contrast to the higher Reynolds number observations of Khalak & Williamson (1999) who observed a peak in $C_{L\,\mathrm{rms}}$ just prior to the maximum response. The high relative magnitude of C_{Lf} at these low Reynolds numbers undoubtedly plays a role in these discrepancies.

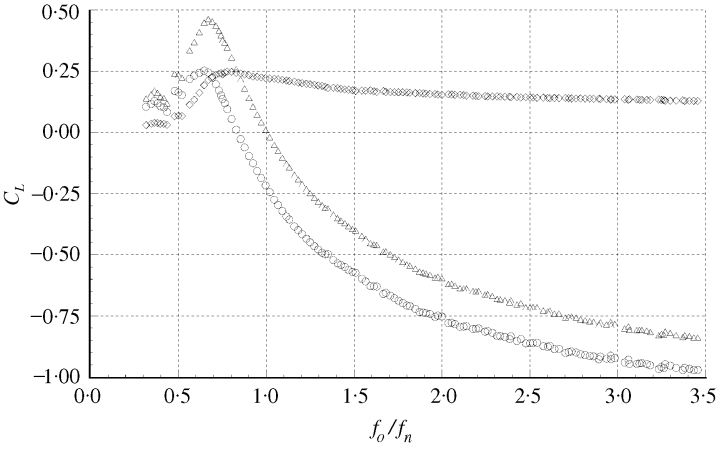

Figure 4. Variation of the component of the lift coefficient, in phase with body displacement, and its constituent parts with oscillatory frequency, for a circular cylinder vibrating freely in the transverse direction, $m^* = 1$, $\beta = 0$: △, C_L; ○, C_{Lp}; ◇, C_{Lf}.

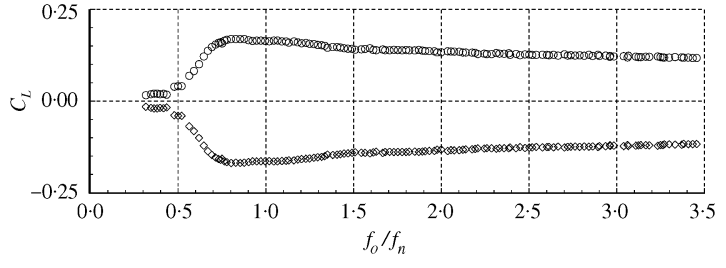

Figure 5. Variation of the constituent parts of the component of the lift coefficient in phase with body velocity with oscillatory frequency for a circular cylinder vibrating freely in the transverse direction, $m^* = 1$, $\beta = 0$: ○, C_{Lp}; ◇, C_{Lf}.

Although C_L must remain entirely in phase or out of phase with y/D since $\beta = 0$, the contributions to C_L from C_{Lp} and C_{Lf} may have components, of equal and opposite sign, in phase with the body velocity (Figure 5). The component of C_{Lp} in phase with velocity provides an excitation force as it remains positive throughout. This is balanced by the equivalent component of C_{Lf} which acts as hydrodynamic damping. The magnitudes of these components are not insignificant in comparison to C_L. The extraordinarily large shear force would appear to be constraining the motion that would otherwise be excited by the considerable component of C_{Lp} in phase with the body velocity.

3.2. Free Transverse Vibrations of a Three-dimensional Flexible Cylinder

The quasi-three-dimensional solver has been used to simulate the flow past a rigid cylinder, length 25 m and aspect ratio 100, subject to a sheared inflow. The inflow Reynolds number is linearly sheared from 200 at its top end to 100 at its bottom end. A particle and lattice image of the wake is shown in Figure 6. Although this figure yields limited insight into the structure of the wake, it demonstrates how the computational method works. Nine equally spaced computational planes are depicted in this figure, each separated by $10D$.

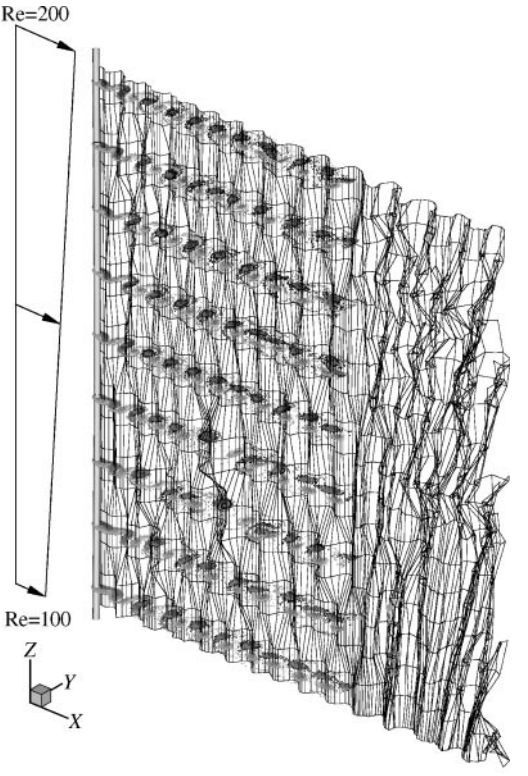

Figure 6. Particle and lattice visualisation of the flow behind a circular cylinder subjected to a sheared onset flow.

Figure 7 displays the spanwise Stouhal number variation as well as the time evolution of the lift coefficient acting on the cylinder. The Strouhal number varies from 0·156 at the low Reynolds number end to 0·185 at the upper end. The time evolution of C_L shows signs of cellular shedding, as has been widely reported for sheared flow. However, one must be cautious in identifying dislocations between such cells, given the coarse nature of the spanwise resolution.

The cylinder was then released and allowed to oscillate freely in the transverse direction, with its ends pinned. The stiffness and applied axial tension are 19·8 MN m^2 and 14·8 MN, respectively. The tension was set deliberately high in order that the fundamental mode be excited. Buoyancy and gravity forces are ignored, and structural damping is set to zero. The mass ratio, $m^* = 2m/\rho D^2$, is 4·26, where m is the mass per unit length of the body.

The response (Figure 8) is close to that of the fundamental mode, except that the peak displacement, 0·36D, is found towards the lower Reynolds number end at $z/D = 44$. The frequency of oscillation, f_o, is 1·05f_n, where f_n is the frequency of the fundamental mode in a vacuum. In contrast with the lower mass ratio case simulated in two dimensions, the structure is dominant in modifying the shedding frequency towards the natural frequency. As indicated by Figure 9, the shedding frequencies at the end points remain relatively unperturbed by the oscillation, whereas those in between are significantly modified.

The lift coefficient evolution (Figure 9) shows significant spanwise correlation between $z/D = 25$ and 75, over which the shedding and oscillatory frequencies remain locked. At the location of the peak response, $z/D = 44$, the C_L evolution shows an abrupt phase change.

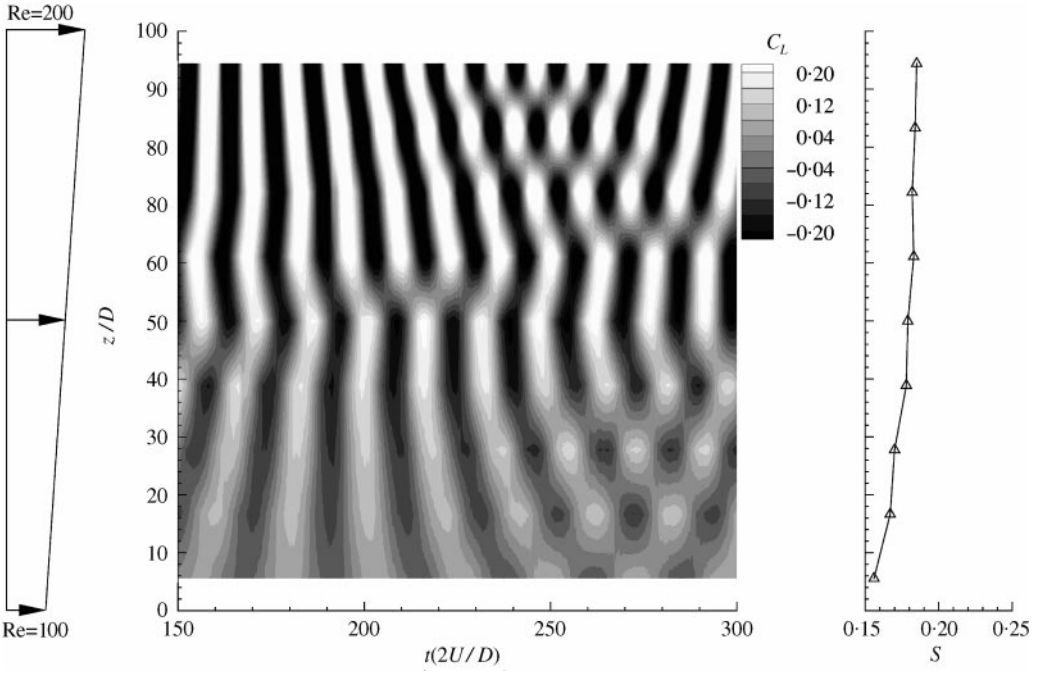

Figure 7. Spanwise Strouhal number, S, variation and time evolution of the lift coefficient, C_L, acting on a stationary circular cylinder subjected to a sheared onset flow.

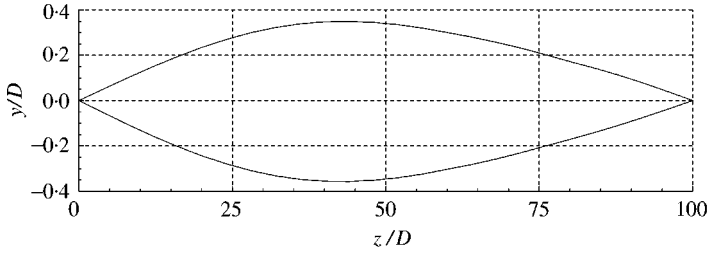

Figure 8. Response envelope of a circular cylinder subjected to a sheared onset flow, vibrating freely in the transverse direction.

On the lower V_r side, $z/D < 44$, C_L and y/D remain in phase; towards the higher V_r end, $z/D > 44$, C_L and y/D are in anti-phase. This phase change is not altogether unsurprising as to some degree it mimics the changes one would expect from a variable reduced velocity.

4. CONCLUSIONS

The low Reynolds number two-dimensional simulations exhibited lock-in throughout. The ability of the fluid at low mass ratios to dominate over the structure in oscillating the body far from its natural frequency was observed. This was facilitated by considerable changes to the added mass. Very high shear stress contributions to the lift force were observed, which

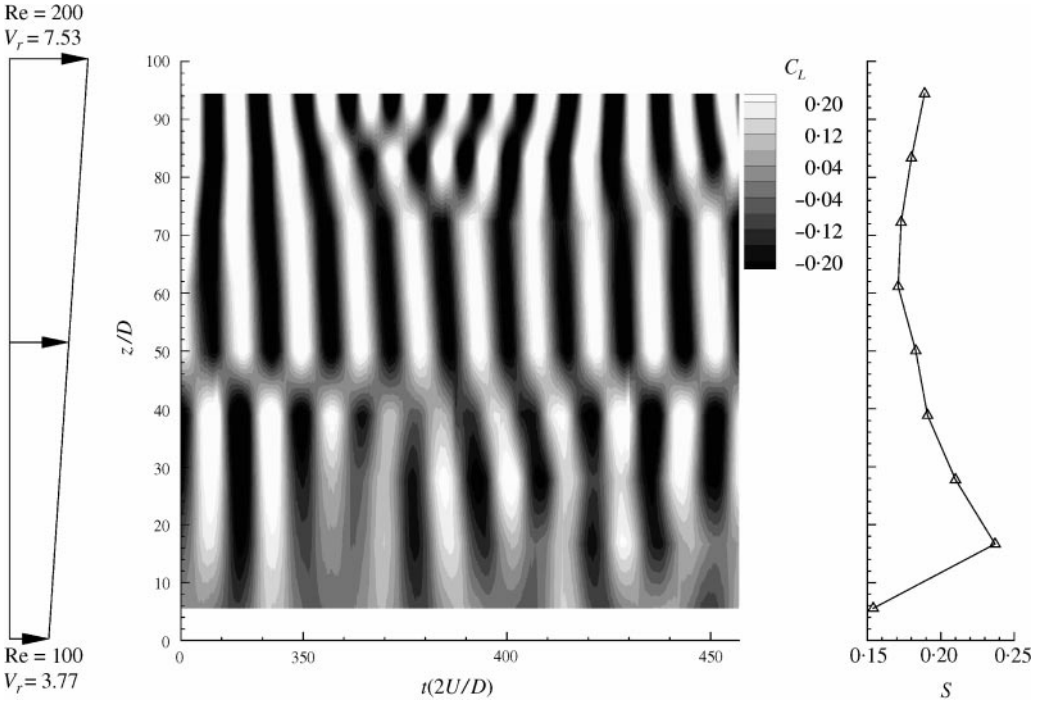

Figure 9. Spanwise Strouhal number, S, variation and time evolution of the lift coefficient, C_L, acting on a transversely oscillating flexible circular cylinder subjected to a sheared onset flow.

undoubtedly play a significant role in the dynamics of the vortex excited cylinder at low Reynolds numbers.

Cellular shedding in the wake of the three-dimensional circular cylinder, when subject to a sheared onset flow, was observed. Despite the shear, the transverse vibrations of the cylinder were seen to correlate the vortex shedding over a substantial proportion of the body's length whilst towards its ends little synchronization was observed.

ACKNOWLEDGEMENTS

The financial support of BP and of the U.K. EPSRC is acknowledged for this work.

REFERENCES

BRIKA, D. & LANEVILLE, A. 1995 The hysteresis and bifurcation phenomena in the aeolian vibrations of a circular cylinder. In *Flow-Induced Vibration* (ed. P. W. Bearman), pp. 27–38, Rotterdam: A. A. Balkema.

GIANNAKIDIS, G. & GRAHAM, J. M. R. 1997 Prediction of the loading on a HAWT rotor including effects of stall. In *EWEC97* (ed. R. Watson), pp. 434–439, Dublin: IWEA.

GRAHAM, J. M. R. 1988 Computation of viscous separated flow using a particle method. In *Numerical Methods for Fluid Dynamics III*, IMA Conference Series **17,** 310–317.

HERFJORD, K., LARSEN, C. M., FURNES, G., HOLMÅS, T. & RANDA, K. 1999 FSI-simulation of vortex-induced vibrations of offshore structures. In *Computational Methods for Fluid-Structure Interaction* (eds T. Kvamsdal *et al.*), pp. 283–303, Trondheim: Tapir.

KHALAK, A. & WILLIAMSON, C. H. K. 1999 Motions, Forces and Mode Transitions in Vortex-Induced Vibrations at Low Mass-Damping. *Journal of Fluids and Structures* **13,** 813–851.

LUCOR, D., EVANGELINOS, C. & KARNIADAKIS, G. E. 2000 DNS-derived force distribution on flexible cylinders subject to VIV with shear flow. In *Flow-Induced Vibration* (eds S. Ziada & T. Staubli), pp. 281–287, Rotterdam: A. A. Balkema.

NEWMAN, D. & KARNIADAKIS, G. E. 1995 Direct numerical simulations of flow over a flexible cable. In *Flow-Induced Vibration* (ed. P. W. Bearman), pp. 193–203, Rotterdam: A. A. Balkema.

WILLDEN, R. H. J. & GRAHAM, J. M. R. 2000 Vortex induced vibration of deep water risers. In *Flow-Induced Vibration* (eds S. Ziada & T. Staubli), pp. 29–36, Rotterdam: A. A. Balkema.